Unsteady flow in a rigid 3-D model of the carotid artery bifurcation

Unsteady Flow in a Rigid 3-D Model of the Carotid Artery Bifurcation

C. C. M. Rindt

A. A. v. Steenhoven

Department of Mechanical Engineering,
Eindhoven University of Technology,
Eindhoven, The Netherlands

In the present study, finite element calculations are performed of blood flow in the carotid artery bifurcation under physiological flow conditions. The numerical results are compared in detail with laser-Doppler velocity measurements carried out in a perspex model. It may be concluded that the numerical model as presented here is well capable in predicting axial and secondary flow of incompressible Newtonian fluids in rigid-walled three-dimensional geometries. With regard to the flow phenomena occurring, a large region with reversed axial flow is found in the carotid sinus opposite to the flow divider. This region starts to grow at peak systole, has its maximal shape at minimal flow rate and totally disappears at the start of the acceleration phase. C-shaped axial velocity contours are formed in the deceleration phase, which are highly influenced by secondary flows. These latter flows are mainly induced by centrifugal forces, flow branching, and tapering of the carotid sinus. Lowering the sinus angle, the angle between the main branch and the carotid sinus, results in a smaller region with reversed axial flow.

Introduction

Knowledge about the flow phenomena occurring in the carotid artery bifurcation is important for several reasons. On the one hand, there is a strong interaction between the flow phenomena occurring and the process of atherogenesis (Caro et al., 1971; Glagov et al., 1988). Atherosclerotic plaque formation, for example, is often found in regions with low shear rates. These regions are often located at the inner bend of curved tubes and at the nondivider walls of bifurcations (Zarins et al., 1983; Ku et al., 1985). On the other hand, detailed information about the flow phenomena occurring may be useful in the detection of atherosclerosis in an early stage of the disease by noninvasive methods like pulsed Doppler (Barnes et al., 1982; Roederer et al., 1984; Ku et al., 1985; Merode et al., 1988). Therefore, detailed insight into the complicated flow fields in bends and bifurcations, the preferential sites of atherosclerosis, and knowledge about the influence of geometrical variations and low grade lesions on the flow patterns, may be important in further development of these methods.

Experiments are successfully employed to get insight into the complex flow patterns occurring in bends and bifurcations (Olson, 1971; Bharadvaj et al., 1982; Cho et al., 1985; Bovendeerd et al., 1987; Ku and Giddens, 1987). A great disadvantage of these methods, however, is their time-consuming character. An alternative approach is the development of numerical models. Many investigators studied unsteady flow in 2-D models of bifurcations (Fernandez et al., 1976; O'Brien et al., 1976; Florian and Perktold, 1982; Perktold and Hilbert, 1986). Accuracy of these models can be estimated by repeating the calculation at different mesh refinements (Vosse et al., 1986). Also experimental methods are used to get an impression of the reliability of the results (Rindt et al., 1987). The last five years also unsteady flow calculations in 3-D models of curved tubes and bifurcations are becoming common practice (Perktold and Resch, 1990; Rindt et al., 1991). However, for these cases mesh refinement is not carried out because of the lack of enough computer power. Therefore, comparison with experiments is still indispensible to get insight into the number of elements and time steps needed to achieve reliable results.

In this study unsteady flow is investigated in a rigid-walled three-dimensional model of the carotid artery bifurcation. Both finite element calculations and laser-Doppler measurements are performed. First, the numerical and experimental methods are described. Because these methods are already described in previous studies only the main characteristics are mentioned. Second, a quantitative comparison is given of the experimental and numerical data, the results of axial and secondary flow are presented as function of time and the influence is studied of a small change in the angle between the main branch and the carotid sinus. Finally, the results are discussed and some conclusions are given.

Methodology

The numerical method used is based on the standard Galerkin finite element method (Cuvelier et al., 1986). A detailed description of the method for the 2-D case is given by Vosse et al. (1986). Rindt et al. (1990) used the same method to calculate steady flow in a 3-D model of the carotid artery bifurcation, whereas Rindt et al. (1991) used the method to describe unsteady entrance flow in a 90-degree curved tube. Blood flow in the present study is supposed to be incompressible, laminar, and Newtonian. The penalty function approach is used to eliminate the pressure from the Navier-Stokes equations. The time-derivatives are discretized by the Crank-Nicolson finite difference scheme which is $O(\Delta t^2)$ accurate in time. One step of a Newton-Raphson iteration scheme is performed to linearize the convective term.

The 3-D element used is the 27-noded Crouzeix-Raviart element consisting of 27 nodes for the velocity (triquadratic) and 1 node for the pressure (piecewise linear). The division of the carotid artery bifurcation into elements is carried out with the mesh generator, as described by Rindt (1989). Figure 1 shows the element division around the flow divider. The number of elements is equal to 1234, whereas the number of nodal points is equal to 11763.

The set of equations is solved in a straight forward manner by Gauss elimination. Because of the enormous amount of computer power needed the calculations are performed on a Cray ymp. One iteration on this machine took about 3 minutes of

Contributed by the Bioengineering Division for publication in the JOURNAL OF BIOMECHANICAL ENGINEERING. Manuscript received by the Bioengineering Division March 19, 1993; revised manuscript received December 17, 1994. Associate Technical Editor: R. Nerem.

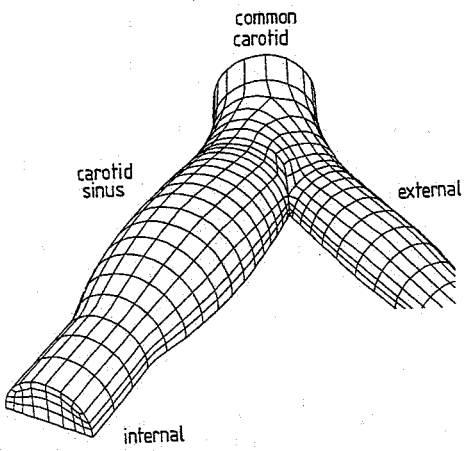

Fig. 1 Element division of the carotid artery bifurcation around the flow divider

CPU time. The package Sepran (Segal, 1984) is used to build and solve the system of equations.

Figure 2 shows the flow rates as function of time through the main branch and both daughter branches as prescribed in the numerical calculations. The Reynolds number, based on the mean velocity through and the diameter of the common carotid artery, at various time intervals is also indicated. The values of the flow rates are derived from experimental data which is elucidated in more detail at the end of this section. To install these flow rates in the calculations the velocities are prescribed at the entrance of the common carotid artery and at the end of the external carotid artery. The velocity fields at these sites are presumed to be fully developed (Womersley profiles). To this purpose, the length of the external carotid artery is chosen to be 7 times the diameter of the common carotid artery. At the outflow section of the internal carotid artery stress-free boundary conditions are prescribed. 2-D calculations showed that this type of boundary condition, which is physically not correct, does not influence the upstream solution for more than one element. The length of the internal carotid artery is chosen to be 3 times the diameter of the main branch. At the rigid wall of the bifurcation the no-slip condition (zero velocities) and in

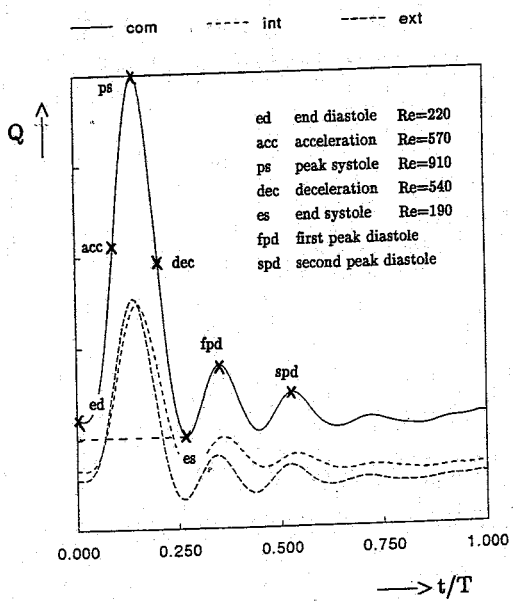

Fig. 2 Flow rates through the main branch and both daughter branches. Also the Reynolds number based on the diameter of and the mean axial velocity through the common carotid artery is indicated.

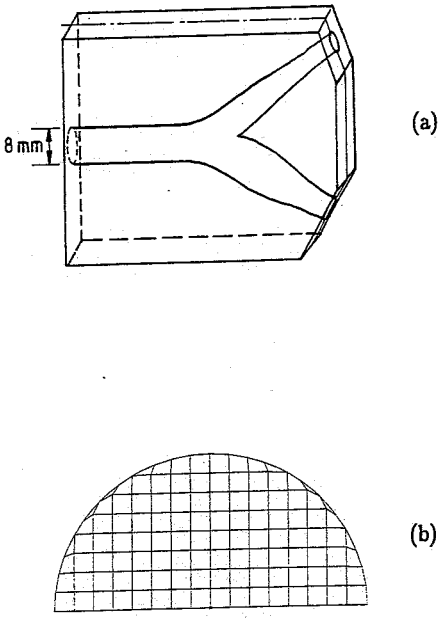

Fig. 3 The perspex model (*a*) and the measuring grid (*b*)

the plane of symmetry the symmetry condition (zero normal velocity and zero tangential stresses) are opposed.

As initial guess for the unsteady flow calculations a steady state solution of diastolic flow is used. One flow pulse is divided into 128 timesteps. The acceleration phase of the systolic phase is calculated twice. The difference between the solutions at peak systole for two successive flow pulses is smaller than one percent of the mean axial velocity. Therefore, 148 timesteps are supposed to be sufficient to reach convergence. One complete calculation took about 8 hours of computing time on a Cray ymp.

The experiments are carried out with a laser-Doppler anemometer. Rindt et al. (1991) gives a detailed description of the fluid circuit employed and the measuring errors involved for laser-Doppler velocity measurements carried out in a 90-degree curved tube. The only difference here with the above mentioned experiments is the use of a potassium thiocyanate solution as measuring fluid, which is less destructive than zinc iodide. In Fig. 3(*a*) the perspex model is presented, as used in the experiments, consisting of two halves of perspex split at the plane of symmetry (Rindt et al., 1988). Measurements of the axial velocity component and the secondary velocity component parallel to the plane of symmetry are performed at three sites in the carotid sinus (I0, I1, I2) and one site in the external carotid artery (E0). All measuring sites are perpendicular to the local axis of the branch. Measuring site I0 is located at the flow divider, site I1 one diameter (of the main branch) downstream of the flow divider (about halfway the carotid sinus) and site I2 two diameters downstream (near the end of the bulb). Measuring site E0 is also situated at the flow divider. The measuring grid at each site is the same as used by Rindt et al. (1991) and is presented in Fig. 3(*b*). Besides, detailed measurements of the axial velocity component are performed in the common carotid artery and in the plane of symmetry of the carotid sinus.

The flow rates as prescribed in the calculations are derived from experimental data. To this purpose the axial velocities at the measuring sites I0, I1, I2, and E0 are integrated in a linear fashion. Because the velocity field in the main branch away from the flow divider is axisymmetric, measurement of the axial velocity component over a diameter line is sufficient to calculate the flow rate through this branch. This flow rate is prescribed as inlet condition for the numerical calculations. The flow rate through the internal carotid artery is defined as the mean of the

flow rates at the three measuring sites (I0, I1, I2) in the carotid sinus. Together with the flow rate through the external carotid artery, derived from laser-Doppler measurements at measuring site E0, the flow division ratio can be determined resulting in the flow rates as depicted in Fig. 2. The mutual difference between the flow rates at the measuring sites I0, I1, and I2 is at most 10 percent of the flow rate at peak systole. This difference is mainly caused by installation errors of the pumping power when starting up a measuring session and by the steep velocity gradients near the flow divider (measuring site I0), resulting in too low velocities at this site when detected with laser Doppler. The mean flow rate through the carotid sinus is also added to the flow rate through the external carotid artery and compared to the one through the main branch (should be equal). The largest difference again occurs at peak systole and is about 10 percent of the flow rate at this time level. However, throughout most of the flow cycle the difference is smaller than 3 percent. For an explanation of this difference, the same reasons hold as given above (installation errors in the pumping power and measuring errors near the flow divider). Because the flow rates through the daughter branches are only used for determination of the flow division ratio instead of the flow rates itself, it is presumed that the differences between the numerically and experimentally installed flow rates are within reasonable limits and not larger than 2 percent of the peak flow rate throughout most of the flow cycle.

Results

In this section, first a comparison between the calculations and the measurements is given on the basis of axial flow in the plane of symmetry and secondary flow at three sites of the carotid sinus. Next, a more detailed description is given of the flow field in the carotid sinus based on the numerical results. Finally, the influence is studied for a smaller angle between the main branch and the carotis sinus.

Comparison With Experiments

In Fig. 4 the axial velocities in the plane of symmetry of the carotid sinus are given for both the calculations and the measurements. The results are presented at five time levels, as indicated in Fig. 2. From this comparison it can be observed that there is a good agreement between the numerics and the experiments.

The largest differences in the axial velocity data occurred at the tapering end of the carotid sinus during the acceleration phase, where the axial velocities determined with LDA are somewhat larger than those determined with FEM. Besides, at end systole the velocity gradients near the divider wall of the carotid sinus determined with FEM are somewhat higher than those determined with LDA between the measuring sites I1 and I2. The former difference is probably mainly caused by small differences in the flow rates. It has to be mentioned that the measuring session of the axial velocity components in the plane of symmetry was completely independent of the measuring sessions of the axial flow fields at the three sites in the carotid sinus, from which the numerical flow rates are derived. The difference in velocity gradients is probably caused by small positioning errors of the measuring volume. In Fig. 5 the secondary velocities parallel to the plane of symmetry at three sites in the carotid sinus are shown for two time levels—peak systole and end systole. From this comparison it can be concluded that also for secondary flow there is a good agreement between the experimental and numerical data. The largest differences in the secondary velocity component occur near the side wall of the carotid sinus. This is probably caused by alignment of the measuring volume in the direction of the highest velocity gradients. The same problems also occurred in the experiments of Rindt et al. (1991) when measuring the secondary velocity component parallel to the plane of symmetry for unsteady flow in a 90-degree curved tube.

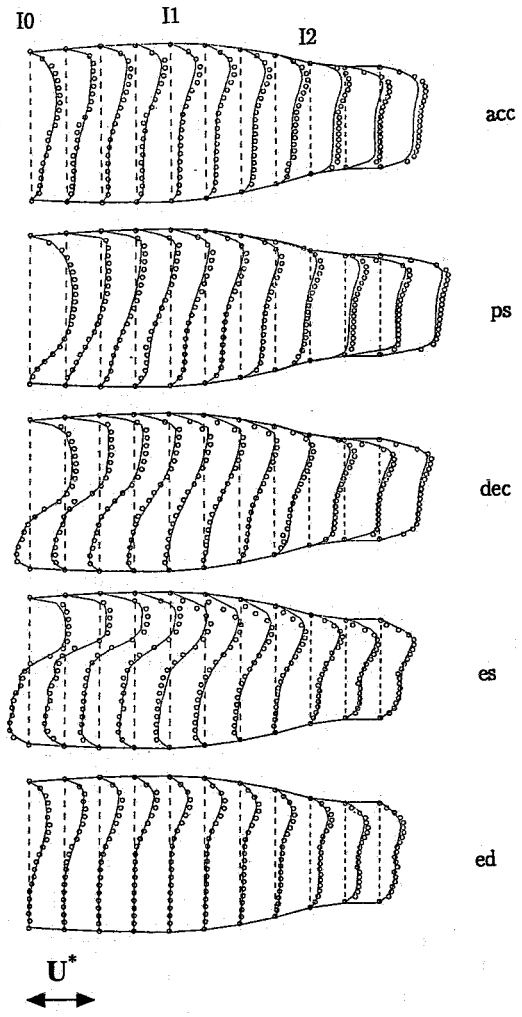

Fig. 4 Comparison between experimental (ooo) and numerical (—) data for axial flow in the plane of symmetry of the carotid sinus. The results are presented at five time levels as indicated in Fig. 2. *U indicates the maximal axial velocity at peak systole in the common carotid artery.**

Axial and Secondary Flow in the Carotid Sinus

Figure 6 shows axial flow in the plane of symmetry of the carotid sinus as function of time. It can be seen that a region with reversed axial flow is starting to develop at peak systole in the most proximal part of the carotid sinus, resulting in a zero velocity gradient at the nondivider wall. This region grows until it reaches its maximal size just before the first peak in diastole (fpd). At this time level the negative axial velocities have about the same magnitude as the positive axial velocities. The largest negative axial velocities occur in the deceleration phase in the proximal part of the carotid sinus. From the first peak toward the second peak in diastole the negative axial velocities are of the same order as the positive axial velocities. After the second peak in diastole towards the end of diastole these negative velocities become almost zero. The region with reversed axial flow is completely washed away at the beginning of the acceleration phase.

In Fig. 7 both axial and secondary flow are presented for four different time levels in the flow cycle. From this figure it can be seen that no region with reversed axial flow is found at peak systole, in accordance with the previous results. This region, however, can be clearly observed in the deceleration phase at

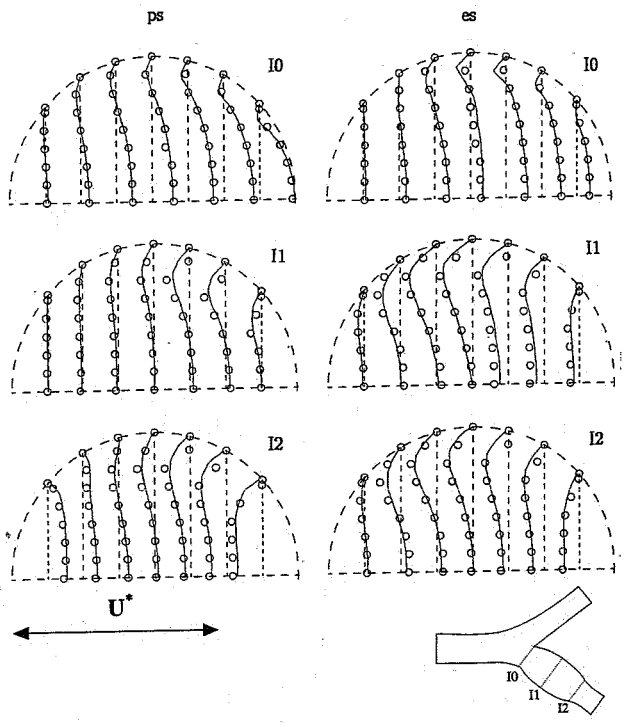

Fig. 5 Comparison between experimental (ooo) and numerical (—) data for the secondary flow component parallel to the plane of symmetry at three sites in the carotid sinus (I0, I1, I2) at two time levels (peak systole, end systole) as indicated in Fig. 2. *U indicates the maximal axial velocity at peak systole in the common carotid artery.**

the sites I0 and I1. At the end systolic phase the reversed flow region at the sites I0 and I1 extends over a large part of the total cross-sectional area. Also, at the tapering end of the carotid sinus a small region with negative axial velocities is found. At end diastole only very small regions with negative axial velocities are observed at the sites I0 and I1 near the nondivider walls. The axial velocity contours at the end systolic phase clearly show the influence of secondary flow on axial flow, resulting in C-shaped contours. High secondary velocities are found during the total deceleration phase. At the end diastolic phase these velocities are low except near the flow divider. The Dean-type vortex, as found for unsteady flow in a 90-degree curved tube (Rindt et al., 1991), is clearly visible at the entrance of the carotid sinus halfway the deceleration phase and at the end systolic phase. Besides, a strong influence of the flow divider and the tapering end of the carotid sinus on the secondary velocities is observed.

Influence of the Sinus Angle

In Fig. 8 the influence is showed of the sinus angle on axial and secondary flow in the carotid bulb for two different time levels. This sinus angle, defined as the angle between the main branch and the carotid sinus, is changed from 25 toward 10 degrees (a change in bifurcation angle from 55 toward 40 degrees). This change in sinus angle results in a smaller region with reversed axial flow and in less C-shaped axial velocity contours at the end systolic phase. Besides, the secondary velocities at site I0, especially those near the flow divider, are smaller for the 10-degree case than for the 25-degree case. The global flow phenomena, however, are only slightly influenced by the sinus angle and the magnitude of the near wall velocities appears to be almost unchanged.

Discussion and Conclusion

One way to make an estimate of the accuracy of numerical results is to do the same calculations at a finer grid and with smaller time steps. However, due to the enormous amount of computer power and computer memory already needed this is not easy to fullfill. For example, one calculation on a Cray ymp took about 8 hours computing time and 250 MByte disk space. Grid refinement of a factor 2 in all three dimensions would increase these numbers to 1000 hours computing time and 10 GByte disk space, supposing that RAM memory is large enough. Therefore, for these kind of calculations experiments are still indispensible. For determination of the number of elements and time steps per period also the experience gained with

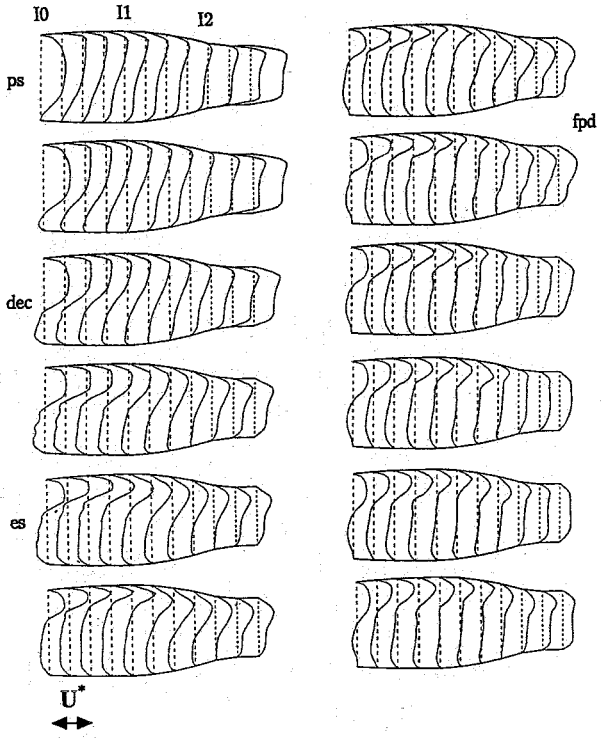

Fig. 6(*a*)

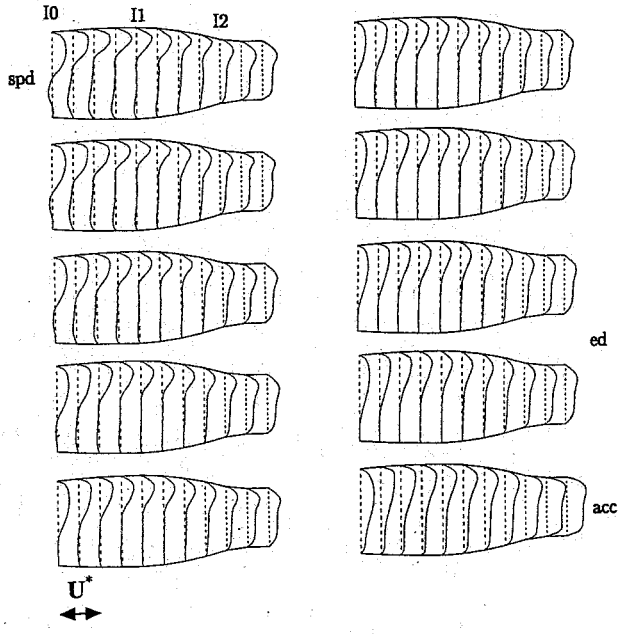

Fig. 6(*b*)

Fig. 6 Numerical results of axial flow in the plane of symmetry as function of time. The time levels are indicated in Fig. 2. *U indicates the maximal axial velocity at peak systole in the common carotid artery.**

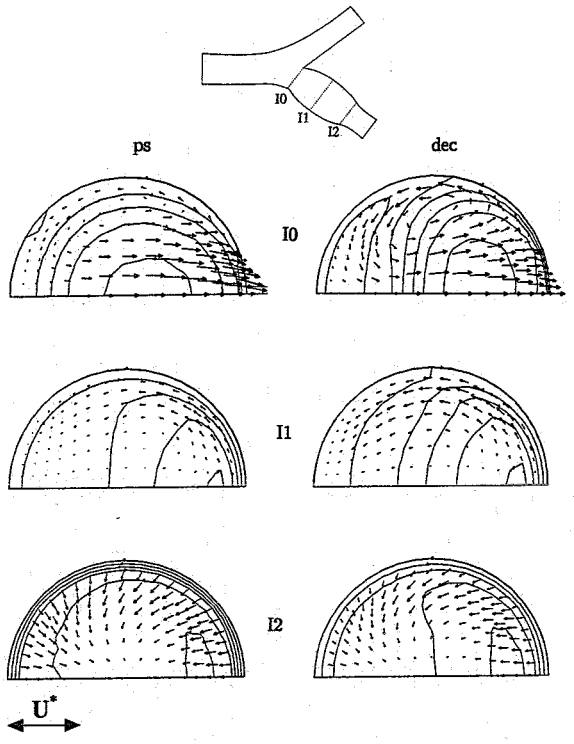

Fig. 7(*a*)

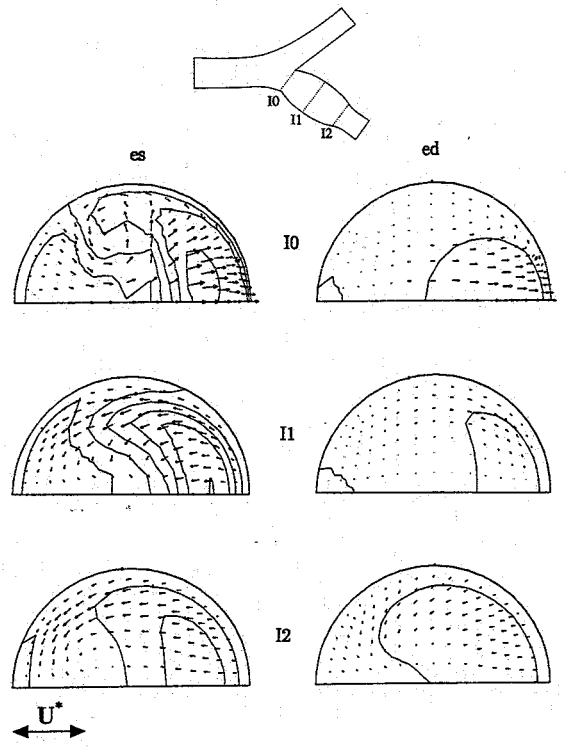

Fig. 7(*b*)

Fig. 7 Numerical results of axial and secondary flow in the carotid sinus at peak systole and halfway through the deceleration phase (*a*) and at both ends of the systolic and diastolic phases (*b*). *U indicates the maximal axial velocity at peak systole in the common carotid artery.**

the steady flow calculations in a 3-D model of the carotid artery bifurcation (Rindt et al., 1990) and with the unsteady flow calculations in a 3-D model of a 90-degree curved tube (Rindt et al., 1991) is used.

From a comparison between the experimental and numerical data it can be concluded that there is a good agreement between both. The largest differences are occurring in the secondary velocity component parallel to the plane of symmetry near the side wall of the perspex model. Like in the 90-degree curved tube (Rindt et al., 1991), this is due to the alignment of the measuring volume in the direction of the highest velocity gradients. Besides, positioning errors play a role here. The somewhat higher axial velocities in the plane of symmetry for the experiments, especially at peak systole, are due to differences in the flow rates.

Detailed analysis of the numerical data revealed good insight into the axial and secondary flow phenomena occurring in the carotid sinus. A region with reversed axial flow is starting to develop at peak systole opposite the flow divider and reaches its largest dimensions just after end systole. At the entrance of the carotid sinus the cross-sectional area of this region is then about 50 percent of the local cross-sectional area. At the beginning of the acceleration phase the region with reversed axial flow is completely "washed away." Most of the time, the highest axial velocities and velocity gradients are found near the divider wall. Due to secondary flow C-shaped axial velocity contours are observed during the second half of the deceleration phase and the first half of the diastolic phase. Secondary flow shows a Dean-type vortex during the deceleration phase in the proximal part of the carotid sinus. More downstream secondary flow is highly influenced by the tapering end of the carotid sinus, resulting in secondary velocities directed toward the center of the tube. For a more extensive description of the flow one is referred to experiments carried out by Bharadvaj et al. (1982), Ku and Giddens (1983), Ku et al. (1985), and Ku and Giddens (1987).

Comparison of these results with the results obtained by Rindt et al. (1990) for steady flow, reveals that the global flow phenomena, like axial flow reversal, C-shaped axial velocity contours and Dean-type vortices, can be distinguished for both flow cases. However, large differences are present in the extent of the region with reversed axial flow, in the pronouncedness of the C-shaped axial velocity contours and in the magnitude and structures of the secondary flow field. The Dean-type vortices and the C-shaped axial velocity contours, due to secondary velocities induced by cetrifugal forces, are also found for unsteady flow in a 90-degree curved tube (Rindt et al., 1991) but are much more pronounced as for unsteady flow in the carotid artery bifurcation.

Comparison of the results with those obtained by Perktold and Resch (1990) reveals a good agreement. Perktold and Resch present the results of a numerical study on unsteady flow in a human carotid artery bifurcation. They studied the influence of the bifurcation angle and the curvedness of the daughter branches on the flow phenomena occurring in relation to atherogenesis. Their numerical model is also based on the Galerkin finite element method but uses a pressure correction scheme instead of a penalty function approach. Besides, they use first order implicit finite differences for time discretization and eight-noded isoparametric brick elements with trilinear velocity functions and piecewise constant pressure for space discretization. It has to be remarked that the number of elements in axial and radial direction is about twice the number of elements used in the present study. The flow division ratio as prescribed by Perktold and Resch (1990) is kept constant as function of time and equal to 70/30 (internal/external). The flow waveform as used by Perktold and Resch differs somewhat from the one used here and is characterized by a "wiggle" in the deceleration phase and only one "clear" peak after minimal flow rate. The peak Reynolds number is somewhat smaller as used in the present study (600 compared to 900). From the four geometries as defined by Perktold and Resch the model named "CAR 2" compares well to the one used here.

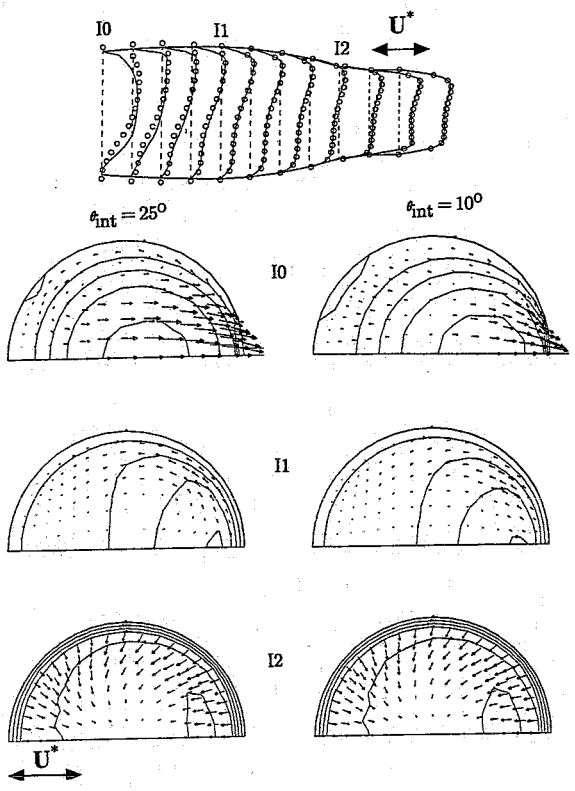

Fig. 8(*a*)

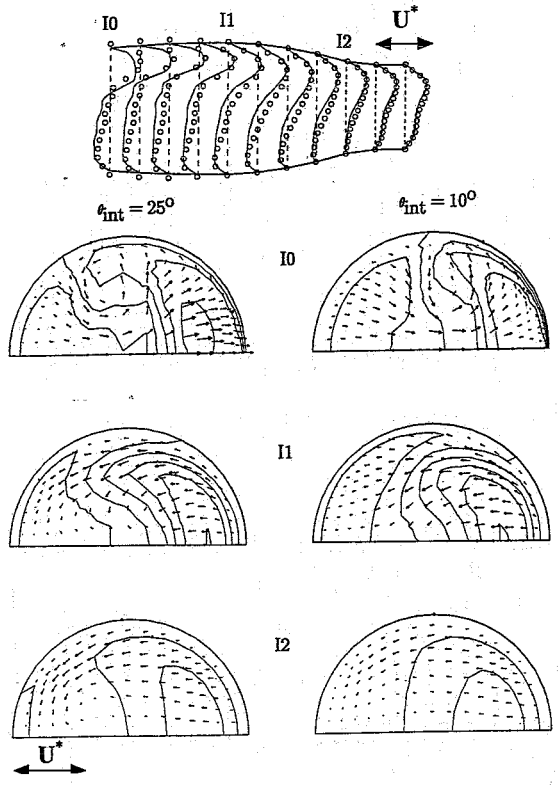

Fig. 8(*b*)

Fig. 8 Numerical results of a comparison between axial and secondary flow in the bulb sinus for a sinus angle of 25 deg (—, left) and 10 deg (ooo, right) at peak systole (*a*) and at end systole (*b*). *U indicates the maximal axial velocity at peak systole in the common carotid artery.**

Despite all the differences mentioned above, the results compare fairly well. Perktold and Resch also observe a start of axial flow reversal at about peak systole. The largest region with axial flow reversal is found at minimal flow rate. Besides, they also observe a large influence of the widening and tapering of the carotid sinus on the secondary flow phenomena, which, on return, results in highly curved axial velocity contours. From this comparison it may be concluded that the global flow phenomena are quite insensitive to relative small changes in the flow waveform, the flow division ratio, and the peak Reynolds number. However, biological variations in all of these parameters are much larger and, therefore, further study is required.

Atherosclerotic plaque formation is often found in low shear regions (Caro et al., 1971; Zarins et al., 1983; Ku et al., 1985). As can be concluded from the results the lowest shear rates occur at the entrance of the carotid bulb opposite to the flow divider throughout the diastolic phase. During this phase the shear rates are opposite to the shear rates at the divider wall. However, in the deceleration phase and at end systole the shear rates are comparable, and still opposite, to the shear rates at the divider wall. In the acceleration phase the shear rates opposite to the flow divider change sign. Therefore, it can be concluded that fluctuating shear rates may play an important role in the process of atherogenesis (Dewey et al., 1981). It has to be mentioned, however, that taking into account flexible walls and non-Newtonian fluid properties may influence the results.

From a diagnostic point of view it is interesting to see that the influence of a change in the sinus angle on the global flow phenomena occurring is small. To use this knowledge in the diagnosis of atherosclerotic plaque formation, however, also the influence of minor stenoses on carotid artery flow has to be investigated. This subject was part of the PhD study of Palmen (1994).

In conclusion, it is remarked that the numerical model as presented here and the model as presented by Perktold and Resch can be used to predict axial and secondary flow in rigid-walled three-dimensional models of the carotid artery bifurcation under the condition that blood behaves like an incompressible and Newtonian fluid. Incorporation of flexible walls is already carried out by Reuderink (1991). Calculations of the flow field in a three-dimensional distensible model of the carotid artery bifurcation yielded a flow field with a global structure equal to the one found in an equivalent rigid model. However, the difference between the wall shear rates at the divider and nondivider walls is reduced by approximately 25 percent. Non-Newtonian behavior of blood is mostly ignored because of the relative large branch diameters resulting in relative high shear rates. However, due to the complex geometry of the carotid artery bifurcation low shear regions are found opposite to the flow divider. Therefore, research on non-Newtonian behavior of blood may be important (Thurston, 1989). Beside these two effects, also the influence of biological variations in the flow waveform, flow division ratio and peak Reynolds number on the flow phenomena occurring has to be studied to get better insight into the process of atherogenesis.

Acknowledgment

This work was sponsored by the Stichting Nationale Computerfaciliteiten (National Computing Facilities Foundation, NCF) for the use of supercomputer facilities, with financial support from the Nederlandse Organisatie voor Wetenschappelijk Onderzoek (Netherlands Organization for Scientific Research, NWO).

References

Barnes, R. W., Rittgers, S. E., and Putney, W. W., 1982, "Real-time Doppler spectrum analysis: predictive value in defining operable carotid artery disease," *Arch. Surg*, Vol. 117, pp. 52–57.

Bharadvaj, B. K., Mabon, R. F., and Giddens, D. P., 1982, "Steady flow in a model of the human carotid bifurcation, Part 1-Flow visualization, Part 2-Laser-Doppler anemometer measurements," *J. Biomech.,* Vol. 15, pp. 349–378.

Bovendeerd, P. H. M., Steenhoven, A. A. v., Vosse, F. N. v. d., and Vossers G., 1987, "Steady entry flow in a curved pipe," *J. Fluid Mech.,* Vol. 177, pp. 233–246.

Cho, Y. I., Back, L. H., and Crawford, D. W., 1985, "Experimental investigation of branch flow ratio, angle, and Reynolds number effects on the pressure and flow fields in arterial branch models," ASME J. BIOCHEM. ENG. Vol. 107, pp. 257–267.

Caro, C. G., Fitz-Gerald, J. M., and Schroter, R. C., 1971, "Atheroma and arterial wall shear," *Proc. Roy. Soc. London,* B, Vol. 177, pp. 109–159.

Cuvelier, C., Segal, A., and Steenhoven, A. A. van, 1986, *Finite element methods and Navier-Stokes equations,* D. Reidel Publishing Comp., Dordrecht.

Dewey, C. F., Bussolari, S. R., Gimbrone, M. A., and Davies, P. F., 1981, "The dynamic response of vascular endothelial cells to fluid shear stress," *J. Biomech.,* Vol. 103, pp. 177–185.

Fernandez, R. C., de Witt, K. J., and Botwin, M. R., 1976, "Pulsatile flow through a bifurcation with applications to arterial disease," *J. Biomech.,* Vol. 9, pp. 575–580.

Florian, H., and Perktold, K., 1982, "Finite Elemente-Computer-Simulation für eine pulsierende StrÖmung in einer arteriellen Verzweigung," *Biomed. Technik,* Vol. 27, pp. 79–84.

Glagov, S., Zarins, C., Giddens, D. P., and Ku, D. N., 1988, "Hemodynamics and Atherosclerosis," *Arch. Pathol. Lab. Med.,* Vol. 112, pp. 1018–1031.

Ku, D. N., and Giddens, D. P., 1983, "Pulsatile Flow in a Model Carotid Bifurcation," *Arteriosclerosis,* Vol. 3, pp. 31–39.

Ku, D. N., Giddens, D. P., Phillips, D. J., and Strandness, D. E., 1985, "Hemodynamics of the normal human carotid bifurcation: in vitro and in vivo studies," *Ultrasound in Med. & Biol.,* Vol. 11, pp. 13–26.

Ku, D. N., and Giddens, D. P., 1987, "Laser Doppler anemometer measurements of pulsatile flow in a model carotid bifurcation," *J. Biomech.,* Vol. 20, pp. 407–421.

Merode, T. van, Hick, P. J. J., Hoeks, A. P. G., and Reneman, R. S., 1988, "The diagnosis of minor to moderate atherosclerotic lesions in the carotid artery bifurcation by means of spectral broadening combined with the direct detection of flow disturbances using a multi-gate pulsed Doppler system," *Ultrasound in Med. & Biol.,* Vol. 14, pp. 459–464.

O'Brien, V., Ehrlich, L. W., and Friedman, M. H., 1976, "Unsteady Flow in a Branch," *J. Fluid Mech.,* Vol. 75, pp. 315–336.

Olson, D. E., 1971, "Fluid mechanics relevant to respiration: flow within curved or elliptical tubes and bifurcating systems," PhD thesis, University of London.

Palmen, D. E. M., 1994, "The influence of minor stenoses on carotid artery flow," PhD thesis, Eindhoven University of Technology, The Netherlands.

Perktold, K., and Hilbert, D., 1986, "Numerical Simulation of Pulsatile Flow in a Carotid Bifurcation Model," *J. Biomed. Eng.,* Vol. 8, pp. 193–199.

Perktold, K., and Resch, M., 1990, "Numerical flow studies in human carotid artery bifurcations: basic discussion of the geometric factor in atherogenesis," *J. Biomed. Eng.,* Vol. 12, pp. 111–123.

Reuderink, P. J., 1991, "Analysis of the flow in a 3D distensible model of the carotid artery bifurcation," PhD thesis, Eindhoven University of Technology, The Netherlands.

Rindt, C. C. M., Vosse, F. N., van de, Steenhoven, A. A. van, Janssen, J. D., and Reneman, R. S., 1987, "A numerical and experimental analysis of the flow field in a two-dimensional model of the human carotid artery bifurcation," *J. Biomech.,* Vol. 20, pp. 499–509.

Rindt, C. C. M., Steenhoven, A. A. v., and Reneman, R. S., 1988, "An experimental analysis of the flow field in a three-dimensional model of the human carotid artery bifurcation," *J. Biomech.,* Vol. 21, pp. 985–991.

Rindt, C. C. M., Steenhoven, A. A. v., Janssen, J. D., Reneman, R. S., and Segal, A., 1990, "A numerical analysis of steady flow in a three-dimensional model of the carotid artery bifurcation," *J. Biomech.,* Vol. 23, pp. 461–473.

Rindt, C. C. M., Steenhoven, A. A. v., Janssen, J. D., and Vossers, G., 1991, "Unsteady entrance flow in a 90° curved tube," *J. Fluid Mech.,* Vol. 226, pp. 445–474.

Roederer, G. O., Langlois, Y. E., Jager, K. A., Primozich, J. F., Beach, K. W., Phillips, D. J., and Strandness, D. E., 1984, "The natural history of carotid arterial disease in asymptomatic patients with cervical bruits," *Stroke,* Vol. 15, pp. 605–613.

Segal, A., 1984, "*Sepran User Manual and Programmers Guide,*" Ingenieurs buro Sepra, Leidschendam.

Thurston, G. B., 1989, "Rheological analogs for human blood in large vessels," *2nd International Symposium on Biofluid Mechanics and Biorheology in Large Blood Vessels,* Munich, June 25–28.

Vosse, F. N. van de, Segal, A., Steenhoven, A. A. van, and Janssen, J. D., 1986, "A finite element approximation of the unsteady 2D-Navier-Stokes equations," *Int. J. Num. Meth. Fluids,* Vol. 6, pp. 427–443.

Zarins, C. K., Giddens, D. P., Bharadvaj, B. K., Sottiurai, V. S., Mabon, R. F., and Glagov, S., 1983, "Carotid bifurcation atherosclerosis: Quantitative correlation of plaque localization with flow velocity profiles and wall shear stress," *Circulation Res.,* Vol. 53, pp. 502–514.